REPORT OF INVESTIGATIONS/1991

Thermal Models of a Flame Arrester

By John C. Edwards

UNITED STATES DEPARTMENT OF THE INTERIOR

BUREAU OF MINES

Mission: As the Nation's principal conservation agency, the Department of the Interior has responsibility for most of our nationally-owned public lands and natural and cultural resources. This includes fostering wise use of our land and water resources, protecting our fish and wildlife, preserving the environmental and cultural values of our national parks and historical places, and providing for the enjoyment of life through outdoor recreation. The Department assesses our energy and mineral resources and works to assure that their development is in the best interests of all our people. The Department also promotes the goals of the Take Pride in America campaign by encouraging stewardship and citizen responsibility for the public lands and promoting citizen participation in their care. The Department also has a major responsibility for American Indian reservation communities and for people who live in Island Territories under U.S. Administration.

Report of Investigations 9378

Thermal Models of a Flame Arrester

By John C. Edwards

UNITED STATES DEPARTMENT OF THE INTERIOR
Manuel Lujan, Jr., Secretary

BUREAU OF MINES
T S Ary, Director

Library of Congress Cataloging in Publication Data:

Edwards, John C.
Thermal models of a flame arrester / by John C. Edwards.

p. cm. — (Report of investigations / United States Dept. of the Interior, Bureau of Mines; 9378)

Includes bibllographical references (p. 15).

Supt. of Docs. no.: I 28.23:9378.

1. Mine explosions—Prevention. 2. Mine fires—Prevention and control. 3. Heat—Transmission—Mathematical models. I. Title. II. Series: Report of investigations (United States. Bureau of Mines); 9378.

TN23.U43 [TN313] 622 s—dc20 [622'.82] 91-10810 CIP

CONTENTS

ILLUSTRATIONS

TABLES

UNIT OF MEASURE ABBREVIATIONS USED IN THIS REPORT

°C	degree Celsius	$g \cdot cm^{-3}$	gram per cubic centimeter
$cal \cdot cm^{-1} \cdot s^{-1} \cdot K^{-1}$	calorie per centimeter per second per kelvin	$g \cdot cm^{-1} \cdot s^{-1}$	gram per centimeter per second
$cal \cdot cm^{-2} \cdot s^{-1} \cdot K^{-4}$	calorie per square centimeter per second per kelvin to the fourth power	$g \cdot mol^{-1}$	gram per mole
		in	inch
$cal \cdot g^{-1} \cdot K^{-1}$	calorie per gram per kelvin	$in^2 \cdot ft^3$	square inch per cubic foot
$cal \cdot mol^{-1} \cdot K^{-1}$	calorie per mole per kelvin	K	kelvin
cm	centimeter	$kcal \cdot g^{-1}$	kilocalorie per gram
cm^3	cubic centimeter	mbar	millibar
$cm \cdot s^{-1}$	centimeter per second	mm	millimeter
$cm^2 \cdot cm^{-3}$	square centimeter per cubic centimeter	μm	micrometer
		ms	millisecond
$cm^3 \cdot K^{-1} \cdot cal^{-1}$	cubic centimeter per kelvin per calorie	μs	microsecond
$cm^2 \cdot s^{-1}$	square centimeter per second	$m \cdot s^{-1}$	meter per second
$dyn \cdot cm^{-2}$	dyne per square centimeter	psi	pound (force) per square inch
$erg \cdot mol^{-1} \cdot K^{-1}$	erg per mole per kelvin	psig	pound (force) per square inch, gauge
ft^3	cubic foot		
g	gram	s	second

THERMAL MODELS OF A FLAME ARRESTER

By John C. Edwards[1]

ABSTRACT

To increase the capability to predict the effectiveness of a flame arrester in the cooling of hot combustion gases expelled through a flame arrester, the U.S. Bureau of Mines developed an equilibrium model and one- and three-dimensional transient thermal models of a flame arrester, which were used to predict the temperature evolution within the arrester and the maximum temperature at the external surface of the arrester. The models account for convective and conductive heat transport within the arrester and radiative losses at the exit surface. The gas flow through the arrester is established from an empirically derived relationship between the gas velocity and the pressure gradient across the arrester. Lateral heat loss from the arrester to the enclosure wall is accounted for in the three-dimensional model. The model calculations for maximum outside surface temperature of the arrester showed an approximate agreement with measured values for vent-area-to-enclosure-volume ratios between 12 and 28 $in^2 \cdot ft^{-3}$.

[1]Research physicist, Pittsburgh Research Center, U.S. Bureau of Mines, Pittsburgh, PA.

INTRODUCTION

As part of the U.S. Bureau of Mines research program directed toward the improvement of electrical safety and the utilization of permissible equipment in mines, several thermal models of a flame arrester were developed to establish criteria for the safe venting of hot combustion gases from an electrical enclosure. Without the availability of venting, heavy and bulky enclosures are required to withstand the internal gas pressure increase associated with a methane (CH_4) and air or coal dust and air explosion (*1*).[2] A confined stoichiometric CH_4-air explosion could achieve a pressure in excess of 100 psi. Venting alleviates the internal gas pressure increase and permits the use of lighter weight, less bulky enclosures. Simultaneously, the vent is expected to quench the flame front associated with the explosion so as to preclude propagation of the explosion into a combustible CH_4 or coal dust environment that might exist external to the enclosure. The presence of a flame arrester in the vent opening is effective in quenching the flame. An early exposition of the industrial use of flame arresters and their advantages and disadvantages outlines a basic specification procedure for the implementation of flame arresters (*2*). A flame arrester will structurally be composed of either wire gauze, crimped ribbon, or an open cellular metal foam. Experimental studies were made of the effectiveness of an open-cell metal foam as an arrester (*3-4*). The foam used was RETIMET,[3] a registered trademark of Dunlop Ltd. of Coventry, Warwickshire, England; it was tested (*3*) as a flame arrester for CH_4-air explosions in a 1/2-ft^3 enclosure with vent-area-to-enclosure-volume (A/V) ratios between 12 and 28 $in^2 \cdot ft^{-3}$. Additional tests were made at the Bureau (*4*) for a vent- area-to-enclosure-volume ratio of 54 $in^2 \cdot ft^{-3}$. The larger the vent-area-to-enclosure-volume ratio, the greater the reduction in the maximum gas pressure in the enclosure and the greater the reduction in the external surface temperature of the arrester.[4] Studies (*5-7*) have been made of the effect of vent size on pressure venting. These studies do not take into consideration the presence of an arrester in the vent. An important design criterion for arrester deployment is not only how to quench the flame and prevent its transmission into the external environment, which will most probably contain the same combustible mixture as in the enclosure, but also how to adequately cool the expelled gases so as not to heat the arrester external surface in excess of the autoignition temperature of any combustible material in contact with the arrester. The autoignition temperature for a stoichiometric CH_4-air mixture is approximately 605° C (*8*), while for a layer of coal dust in contact with a heated surface, the autoignition temperature can be as low as 160° C (*9, p. 51*). The autoignition temperature for a coal dust layer depends upon the dust volatile content, layer thickness, and particle size.

In order to understand the significant parameters in arrester design that control the heat loss from the hot gases expelled through the arrester, several mathematical models of heat and mass transport through porous structures were developed. In general, these are numerical models that require the solution of time- and space-dependent partial differential equations. As a foundation for these complex approaches, a simple equilibrium model was developed first.

EQUILIBRIUM MODEL

For an explosion vented through an arrester, a determination can be made of the maximum temperature the arrester will achieve based upon the first law of thermodynamics. In consideration of the experimental studies of the venting of an explosion through a combination of metal screens and arresters (*3*), both components are included in this model. The primary model consideration is that the thermal energy released by the CH_4-air explosion in the enclosure is transferred to the screens and the arrester to the extent that thermal equilibrium occurs between the product gases, the screens, and the arrester. If the combustion enclosure contains a mass of CH_4 m_{CH_4} and a mass of air m_a at an ambient temperature T_0, the flame temperature T_f of the combustion products is determined from a constant volume T_s calculation. The initial CH_4-air mixture results in the following reaction between the CH_4 with the oxygen (O_2) in the air to produce carbon dioxide (CO_2) and water vapor (H_2O):

$$CH_4 + 2O_2 \rightarrow CO_2 + 2H_2O. \qquad (1)$$

T_f is determined from an application of the first law of thermodynamics to equation 1 for the condition of stoichiometry or excess air.

[2]Italic numbers in parentheses refer to items in the list of references preceding the appendixes at the end of this report.

[3]Reference to specific products does not imply endorsement by the U.S. Bureau of Mines.

[4]In this report, the temperature at the arrester external surface will refer to the gas and the arrester unless otherwise specified.

$$m_{CH_4}\Delta H_c = (m_{CO_2}C_{V_{CO_2}} + m_{H_2O}C_{V_{H_2O}} + (m_a - m_{O_2})C_{V_a})(T_f - T_0), \quad (2)$$

where $C_{V_{CO_2}}$, $C_{V_{H_2O}}$, and C_{V_a} are the constant volume high-temperature specific heats of CO_2, H_2O, and air, respectively, and ΔH_c is the constant volume heat of combustion. The mass of CO_2 and H_2O produced are denoted by m_{CO_2} and m_{H_2O}. The O_2 depleted from the air in the reaction is denoted by m_{O_2}.

Equation 2 is rewritten for the temperature increase of the product gas in terms of the mass fraction f of CH_4 to air, $f = m_{CH_4}/m_a$.

$$T_f - T_0 = f\Delta H_c / [f(a_{CO_2}C_{V_{CO_2}} + a_{H_2O}C_{V_{H_2O}} - a_{O_2}C_{V_a}) + C_{V_a}], \quad (3)$$

where a_k is the ratio of mass of species k, m_k, to m_{CH_4} for species ($k = CO_2$, H_2O, and O_2). The combustion temperature T_f, as well as the composition and heat capacity of the product gases, will be determined by whether the initial CH_4-air mixture is stoichiometric or CH_4 lean.

In the absence of heat loss to the enclosure walls, a determination of the final equilibrium temperature T_1 of gas, screens, and arrester can be made. If there are a number of screens n, each of screen mass m_s, and an arrester of mass m, then T_1 is determined as follows:

$$T_1 = T_0 + m_a f\Delta H_c / [m_a f(a_{CO_2}C_{V_{CO_2}} + a_{H_2O}C_{V_{H_2O}} - a_{O_2}C_{V_a}) + m_a C_{V_a} + nm_s C_{p_1} + mC_{p_s}], \quad (4)$$

where C_{p_1} = constant pressure specific heat of screen,

and C_{p_s} = constant pressure specific heat of arrester.

The mass of air m_a contained in the volume V of the enclosure is determined from the molar relationship for a gas composed of a mixture of CH_4 of molecular weight W_{CH_4} and air of molecular weight W_a at ambient temperature T_0.

$$V = (m_{CH_4}/W_{CH_4} + m_a/W_a)(22.4 \times 10^3)\left(\frac{T_0}{273}\right). \quad (5)$$

Rearrangement of the terms in equation 5 yields

$$m_a = \frac{10^{-3}}{22.4}\frac{V}{f/W_{CH_4} + 1/W_a}\left(\frac{273}{T_0}\right). \quad (6)$$

For arrester design purposes, it is useful to characterize the arrester in terms of its fundamental physical and geometric properties.

The mass of the arrester m is determined from the arrester's porosity ϵ, bulk density ρ_s, thickness ℓ, and cross-sectional area A.

$$m = (1 - \epsilon)\rho_s A\ell. \quad (7)$$

The mass of a screen m_s is determined from the screen's porosity ϵ_s, bulk density σ_s, wire diameter d, and cross-sectional area A_s. For an interwire separation distance ℓ_s, within each screen, ϵ_s can be developed from geometric arguments.

$$\epsilon_s = 1 - \frac{\pi}{4}\cdot\frac{d(2\ell_s + d)}{(\ell_s + d)^2}. \quad (8)$$

The screen mass is

$$m_s = (1 - \epsilon_s)\sigma_s dA_s. \quad (9)$$

Equations 1 through 9 were used to determine the maximum arrester temperature with and without screens. Each screen, in accord with previous research (*2-3*), was assumed to be 20 mesh and composed of stainless steel. Table 1 is a listing of the physical properties of the screens and the arrester, as well as the thermodynamic properties of the gases. The RETIMET flame arrester is a highly porous metal foam with a porosity in excess of 0.9 and a mass density characteristic of the primary metal constituent nickel. For the values shown, the screen porosity ϵ_s was determined to be 0.54.

Table 2 shows the calculated maximum equilibrium temperature T_1 for several values of cross-sectional area of arrester A and CH_4-air mass fraction f. Values of A were selected for arrester sizes that would be used in the vent of an electrical box in a mine. For a 6-in by 6-in vent, the arrester mass m is 134 g and the screen mass m_s is 39 g, and for a 10-in by 15-in vent, m is 560 g and m_s is 164 g. The value f = 0.0581 represents stoichiometric CH_4-air. The slightly lower f value of 0.041 shows the effect of a reduction in CH_4 concentration. For each of the cases shown in table 2 for stoichiometric CH_4-air, T_1 of the arrester is significantly higher than the autoignition temperature of 605° C reported for CH_4-air (*8*) and considerably higher than the ignition temperature of 160° C reported for coal dust (*9*). For the lower mass fraction, T_1 was reduced, but still was in excess of the ignition temperature for a combustible CH_4-air or coal dust-air mixture. In each case, the presence of screens moderates T_1. A significant increase in the thickness ℓ of the arrester would moderate T_1 at the expense of an

increased flow resistance to the expelled gas, thereby compromising the structural integrity of the enclosure in its ability to withstand a large pressure rise. An alternative is to increase A.

Table 1.—Physical properties of screens, RETIMET flame arrester, and gases

Screens:		
C_{p_1}	$cal \cdot g^{-1} \cdot K^{-1}$	0.1
d	cm	0.046
ℓ_s	cm	0.084
σ_s	$g \cdot cm^{-3}$	8.02
Arrester:		
C_{p_s}	$cal \cdot g^{-1} \cdot K^{-1}$	0.158
ℓ	cm	1.3
ϵ		0.95
ρ_s	$g \cdot cm^{-3}$	8.9
λ_s	$cal \cdot cm^{-1} \cdot s^{-1} \cdot K^{-1}$	2.39×10^{-6} T
Gases:		
a_{CO_2}		2.75
a_{H_2O}		2.25
a_{O_2}		4.0
C_{V_a}	$cal \cdot g^{-1} \cdot K^{-1}$	0.24
$C_{V_{CO_2}}$	$cal \cdot g^{-1} \cdot K^{-1}$	0.29
$C_{V_{H_2O}}$	$cal \cdot g^{-1} \cdot K^{-1}$	0.57
$C_{V_{O_2}}$	$cal \cdot g^{-1} \cdot K^{-1}$	0.22
W_a	$g \cdot mol^{-1}$	29
W_{CH_4}	$g \cdot mol^{-1}$	16
ΔH_c	$kcal \cdot g^{-1}$	11.95
λ_g	$cal \cdot cm^{-1} \cdot s^{-1} \cdot K^{-1}$	$3.5 \times 10^{-6}\sqrt{T}$

The equilibrium model is an overly conservative analysis of the predicted maximum temperature of the arrester. There is, in fact, an important mode of heat loss that occurs through radiation at the external surface of the arrester. This is a primary consideration for the transient models presented in the subsequent sections.

Table 2.—Calculated maximum temperature of arrester from equilibrium model

A	n	T_1, K	T_1, °C
f = 0.041; T_f = 2,002 K			
6 by 6 in	0	1,738	1,465
	1	1,698	1,425
	2	1,660	1,387
	3	1,625	1,352
10 by 15 in	0	1,263	990
	1	1,191	918
	2	1,130	857
	3	1,076	803
f = 0.0581; T_f = 2,564 K			
6 by 6 in	0	2,224	1,951
	1	2,173	1,900
	2	2,124	1,851
	3	2,077	1,804
10 by 15 in	0	1,603	1,330
	1	1,508	1,235
	2	1,427	1,154
	3	1,355	1,082

ONE-DIMENSIONAL TRANSIENT THERMAL MODELS

GAS AND ARRESTER TEMPERATURE IN LOCAL EQUILIBRIUM

If, during expulsion of the hot combustion gas through the arrester, significant heat conduction to the walls of the explosion-proof box is absent, then a one-dimensional heat transfer model can be used to predict the evolution of the arrester temperature. Figure 1 shows a schematic of the arrester that has a thickness ℓ. Hot combustion products at a flame temperature T_f and gas pressure in the enclosure (explosion-proof box) P_2 are expelled at a superficial gas velocity v through the arrester to the external environment, which remains at a pressure P_1. The assumption is made that the heat transfer rate between the gas and the arrester elements is sufficiently fast, such that the gas and the arrester are in local thermal equilibrium defined by a unique temperature T(x,t) at location x and time t. An element of the arrester is understood to be a fiber of gauze, a segment of crimped ribbon, or a segment of the cellular foam structure. The temperature satisfies an energy transport equation:

$$\frac{\partial T}{\partial t} = \alpha_0 \frac{\partial^2 T}{\partial x^2} - \beta_0 \rho_g C_{p_g} v \frac{\partial T}{\partial x}, \qquad (10)$$

where v = superficial gas velocity,

λ_s = arrester thermal conductivity,

C_{p_g} = constant pressure specific heat of gas,

and ρ_g = gas density.

The thermal diffusivity α_0 and parameter β_0 are defined as

$$\alpha_0 = \lambda_s \beta_0 \text{ and}$$

$$\beta_0 = 1/(\epsilon \rho_g C_{p_g} + (1 - \epsilon) \rho_s C_{p_s}).$$

The first term on the right side of equation 10 represents the thermal conduction through the arrester and the second term represents the thermal convection of the product gases.

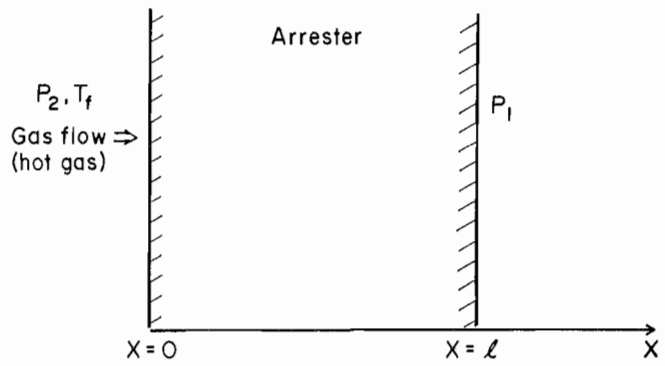

Figure 1.—Schematic of one-dimensional flame arrester of thickness ℓ.

The thermal conductivities are temperature dependent. The values for RETIMET flame arrester, thermal conductivity λ_s, and for the gas thermal conductivity λ_g are listed in table 1. A constant value of 0.31 cal·g^{-1}·K^{-1} is used for the constant pressure specific heat of gas C_{p_g}. The local gas density ρ_g in the arrester is determined from the gas pressure P (in dynes per square centimeter) internal to the arrester and the local temperature T (in kelvins) through the ideal gas law.

$$\rho_g = \frac{W_g}{R_g}\frac{P}{T}, \tag{11}$$

where W_g = gas molecular weight

and R_g = molar gas constant
$(8.3143 \times 10^7$ erg·mol^{-1}·K$^{-1})$.

The superficial gas velocity v is uniquely determined at any time from the gas pressure gradient across the arrester. This determination for RETIMET flame arrester is based upon a correlation between the pressure differential across a 10-mm-thick RETIMET flame arrester and the measured gas flow provided by the manufacturer, as shown in table 3. The manufacturer's data states that the pressure drop ΔP across the arrester increases as the 1.7th power of the gas flow. A regression of the data in table 3, based upon the 1.7th power law, determines the following relationship between $\Delta P = P_2 - P_1$, in millibars, and v, in meters per second, for an arrester 10 mm thick.

$$\Delta P = 0.298v^{1.7}. \tag{12}$$

Figure 2 shows a comparison of the manufacturer's measurements with the predictions based upon equation 12. For a RETIMET flame arrester of thickness ℓ (centimeters) the above expression is modified to read

$$\Delta P/\ell = 0.298v^{1.7}. \tag{13}$$

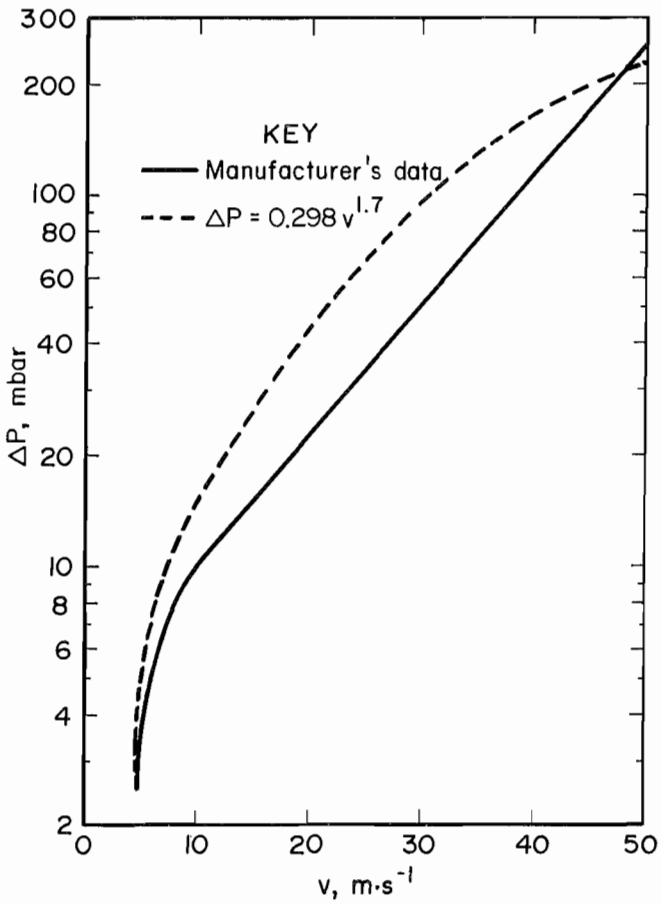

Figure 2.—Pressure drop ΔP across flame arrester versus superficial gas velocity.

Table 3.—RETIMET flame arrester (grade 45, 10-mm-thick) gas flow-pressure data

Gas flow, m·s^{-1}	*Pressure loss, mbar*
1.0	0.15
1.78	.5
5.0	2.5
10.0	10.0
30.0	50.0
50.0	250.0

Source: Dunlop Ltd., Aviation Div., Coventry, Warwickshire, England.

The model transport equation, equation 10, determines a unique solution for specified initial and boundary values for temperature T. The initial value throughout the arrester is the ambient temperature T_0. Boundary values are specified for the arrester internal and external surface. Internal to the enclosure, the arrester surface temperature is identified with the flame temperature T_f, until sufficient hot gas is expelled through the enclosure to equilibrate the gas pressure P internal and external to the arrester, at

which time an adiabatic boundary condition is imposed. Expansion of the combustion gas in the enclosure results in negligible change in T_f. On the external surface of the arrester, energy lost by radiation determines the arrester surface temperature.

The radiation-controlled boundary condition at the external surface balances the internal heat conduction with the radiation cooling.

$$-\lambda_s \frac{\partial T}{\partial x} = e\sigma (T^4 - T_0^4) \qquad (14)$$

at $x = \ell$,

where σ = Stefan-Boltzmann constant (1.3551×10^{-12} cal·cm^{-2}·s^{-1}·k^{-4}),

and e = emissivity (absorptivity) of the arrester surface.

For these considerations, the arrester was assigned an emissivity e of unity as an approximation for an oxidized metal.

The model equations, 10 through 14, are nonlinear because of the temperature-dependent thermal conductivity and radiative cooling boundary condition. In addition, the convective superficial gas velocity v is a generalized function of time t that must be specified for a given application. For these reasons, a numerical procedure was adapted to generate a solution to the model equation. A finite difference procedure that is implicit in time and central in space was well suited for this purpose. The resultant coupled, nonlinear algebraic equations were coded into a FORTRAN computer program that determines the evolution of the arrester temperature through an application of the Thomas algorithm (*10*).

The resultant model was applied to an analysis of a flame arrester project (*3*) that evaluated maximum combustion gas pressure P and maximum interior and exterior surface temperatures of the arrester for four vent-area-to-enclosure-volume ratios between 12 and 28 in^2·ft^{-3}, as shown in table 4. In each case, the 1/2-ft^3 enclosure contained a combustible CH_4-air mixture, and the RETIMET flame arrester was 1/2-in thick, grade 45. A decrease in the vent-area-to-enclosure-volume ratio is associated with an increase in the maximum gas pressure P in the enclosure. As expected, the maximum outside surface temperature of the arrester is lower for the case of a 28 in^2·ft^{-3} vent-area-to-enclosure-volume ratio than for the 12 in^2·ft^{-3} case. The reported relative maximum temperatures are unexpected for the intermediate cases of 24 and 20 in^2·ft^{-3}, in sofar as the maximum temperature does not decrease monotomically with increasing vent area.

Table 4.—Measured maximum gas pressure and maximum surface temperature of RETIMET flame arrester for vent-area-to-enclosure-volume (A/V) ratios between 12 and 28 in^2·ft^{-3}

A/V, (in^2·ft^{-3})	Maximum pressure, psig	Maximum interior surface temperature, °C	Maximum exterior surface temperature, °C
12	1.3	1,138	358
20	.52	961	164
24	.32	970	220
28	.37	1,001	194

Computational simulations were made with the one-dimensional transient thermal model based upon the reported maximum pressure, an assumed gas pressure P decay time t of 300 ms, and the reported maximum inside surface temperature of the arrester for measured values of flame temperature T_f. The selection of the same 300-ms time constant for each of the four cases is somewhat arbitrary, although within the time frame of 1 s expected for expulsion of vented gases. The selection of this time constant serves to demonstrate the utility of the model. These measured values of T_f are considerably lower than adiabatic T_f and only represent the maximum temperature calculated without information regarding the gas temperature T_g evolution. Predicted and measured maximum outside surface temperatures of the arrester for each of the four cases are shown in figure 3. The straight-line segments shown in figure 3 are drawn to clarify the measured and predicted values. A linear interpretation is not implied. An approximate agreement occurs between theory and measurement, although the theory presents a conservative overestimate of the maximum outside surface temperature. These results would exhibit a closer agreement for a decay time less than 300 ms.

The moderating influence of radiation cooling upon the maximum external surface temperature was examined. For a vent-area-to-enclosure-volume ratio of 12 in^2·ft^{-3}, the predicted maximum outside surface temperature of the arrester was 551° C, in comparison to a measured value of 358° C. A repetition of the calculation with the replacement of the radiation boundary condition, equation 13, by an adiabatic boundary condition resulted in an elevated predicted maximum outside surface temperature of 780° C. This demonstrates the importance of radiative cooling as the dominant mode of heat loss.

The one-dimensional transient thermal model defined by equations 10 through 15 appears satisfactory for the analysis of an arrester temperature if the gas pressure history within the enclosure is known. There are two model assumptions that must be considered for completeness. One assumption is the identification of the local gas temperature T_g with the local solid temperature T_s. This

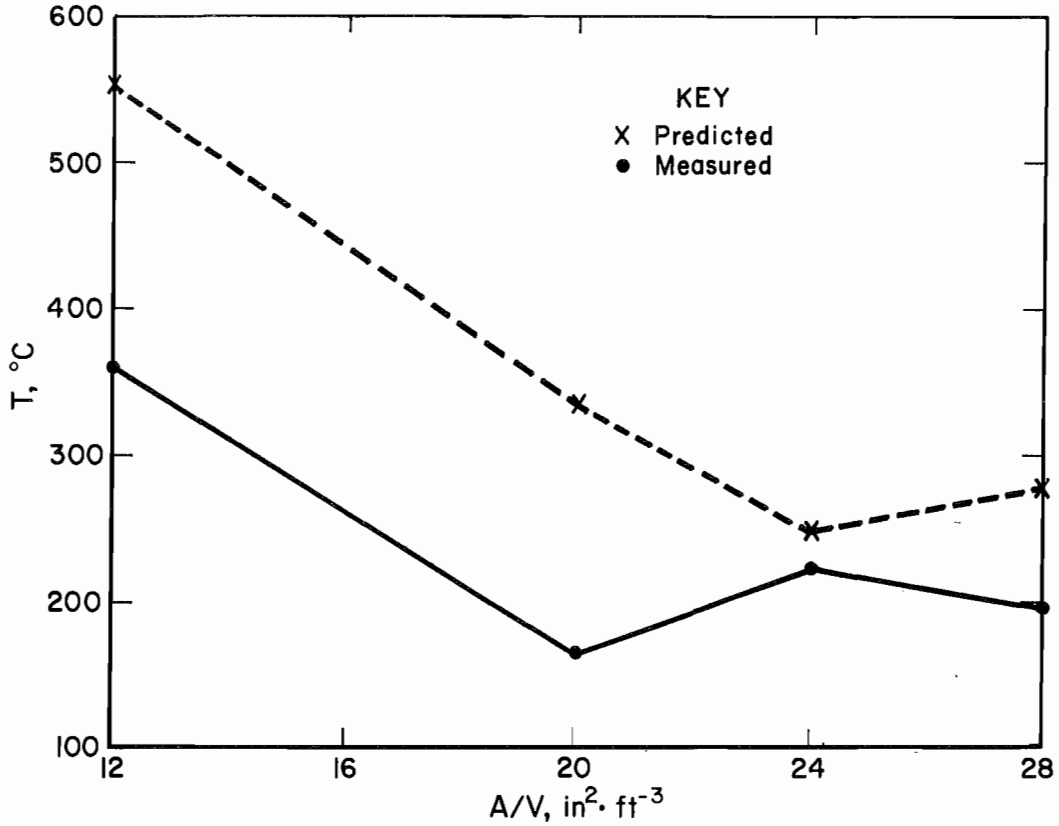

Figure 3.—Measured and predicted maximum outside surface temperatures of arrester for vent-area-to-enclosure-volume (A/V) ratios between 12 and 28 in^2-ft^{-3}.

assumes a thermal equilibration of gas and solid over a time interval significantly smaller than any of the other heat transport processes. This assumption is considered below. The other consideration is the dissipative effect of lateral heat transfer from the arrester to the enclosure walls. This last assumption can only be properly answered with due consideration of a three-dimensional model and will be addressed in the "Three-Dimensional Arrester Transient Thermal Model" section.

GAS AND ARRESTER TEMPERATURE DISTINCT

The one-dimensional model defined by equations 10 through 15 in the previous section assumes that the gas and the arrester are in local thermal equilibrium. This assumption is based upon the expected rapid heat transfer from the gas to the fine mesh structure of the RETIMET metal-foam flame arrester. In order to have an analytic model that can provide a fundamental understanding of the gas-solid heat transfer process, a mathematical model was constructed that decouples the gas temperature T_g and solid temperature T_s through a small, but finite, heat transfer rate between the gas and arrester mesh structure. This model provides an increased capability for the improved design of a flame arrester that increases its efficiency as a thermal sink. As in the previous section, the model is a one-dimensional transient model.

The fundamental heat transport equations for the gas temperature T_g and the solid temperature T_s at a distance x internal to the arrester at time t are two coupled, partial differential equations.

Gas heat transport:

$$\frac{\partial T_g}{\partial t} = \alpha \frac{\partial^2 T_g}{\partial x^2} - \frac{v}{\epsilon} \frac{\partial T_g}{\partial x} - \hat{h} \, (T_g - T_s), \quad (15)$$

Solid heat transport:

$$\frac{\partial T_s}{\partial t} = \alpha_s \frac{\partial^2 T_s}{\partial x^2} + \hat{h}_s (T_g - T_s), \quad (16)$$

where the rate of heat transfer from the gas to the arrester is determined by the coefficient $\hat{h}$,

$$\hat{h} = \frac{h}{\epsilon \rho_g C_{p_g}} S_v, \quad (17)$$

and the rate of heat transfer from the arrester to the gas is determined by the coefficient $\hat{h}_s$,

$$\hat{h}_s = \frac{h}{(1 - \epsilon)\,\rho_s C_{p_s}} S_v, \tag{18}$$

$$\alpha = \frac{\lambda_g}{\epsilon \rho_g C_{p_g}}, \tag{19}$$

The thermal diffusivities α and α_s are defined as

$$\alpha_s = \frac{\lambda_s}{(1 - \epsilon)\,\rho_s C_{p_s}}, \tag{20}$$

where h = gas-solid heat transfer coefficient,

and S_V = arrester-internal-surface-to-volume ratio.

The gas-solid heat transfer coefficient h depends upon the internal mesh structure of the flame arrester.

Two geometrical structures for which gas-solid heat exchange is defined are the cylinder and sphere (*11*). For the model calculations presented herein, the mesh is assumed to be composed of either cylindrical or spherical elements. The gas-solid heat transfer coefficients h for these cases are defined in terms of the Reynolds number Re and Prandtl number Pr, where $Re = D\rho_g v/\mu$, $Pr = C_{p_g}\,\mu/\lambda_g$, μ is the dynamic gas viscosity, and D is the element diameter. For flow past a sphere, h is represented by

$$h = 2\frac{\lambda_g}{D} + 0.6\,\frac{\lambda_g}{D}\,Re^{0.5}\,Pr^{1/3}. \tag{21}$$

For flow past a cylinder, h is represented by

$$h = 0.32\,\frac{\lambda_g}{D} + 0.36\,\frac{\lambda_g}{D}\,Pr^{1/3}\,Re^{0.57}, \tag{22}$$

where the second term is valid for $Re > 100$ (*11*) and the first term is valid for low Re flow (*12*).

The model heat equations 15 and 16 are characterized by four time constants, each of which is associated with a different mode of heat transport.

Gas-solid heat transfer:

$$\tau_1 = (\epsilon \rho_g C_{p_g}/h)/S_v. \tag{23}$$

Convective heat transfer:

$$\tau_2 = \ell/(v/\epsilon). \tag{24}$$

Solid conduction:

$$\tau_3 = (1 - \epsilon)\,\rho_s C_{p_s} \ell^2/\lambda_s. \tag{25}$$

Gas conduction:

$$\tau_4 = \epsilon \rho_g C_{p_g} \ell^2/\lambda_g. \tag{26}$$

The arrester-internal-surface-to-volume ratio (S_V), for grade 45 RETIMET flame arrester is 26 $cm^2 \cdot cm^{-3}$. For a 1/2-in-thick RETIMET flame arrester sample, the time constants were evaluated with the data in table 1 and the temperature-dependent thermal conductivities presented previously. The thermal conductivities were determined at a temperature of 1,840 K, characteristic of a 6.8% CH_4-air combustion temperature T_f. Table 5 lists the evaluation of the time constants. These values show the rate-controlling heat transfer mechanisms, associated with the smallest time constants, to be gas-solid and convective heat transfer.

Table 5.—Thermal time constants

τ_1 .... μs ..	[1]1-1,500
τ_2 .... μs ..	300
τ_3 ..... s ..	30
τ_4 ..... s ..	0.5

[1]Spherical particle diameter between 2 and 2,000 μm.

Equations 15 and 16 are augmented by equations 11 and 13 in order to evaluate the gas density ρ_g and superficial gas velocity v. The internal gas pressure P is assumed to vary linearly across the arrester.

The boundary condition at x = 0 is specified by setting the gas temperature T_g and solid temperature T_s equal to the combustion temperature T_f of CH_4-air mixture until a gas pressure relaxation time τ has elapsed, such that the pressure differential across the arrester vanishes. For time t greater than τ, an adiabatic condition is imposed at x = 0 on both T_g and T_s. These conditions are expressed as

$$T_g = (0, t) = T_s(0, t) = T_f, t < \tau, \tag{27}$$

$$\left.\frac{\partial T_g}{\partial x}\right|_{x=0} = \left.\frac{\partial T_s}{\partial x}\right|_{x=0} = 0, t > \tau. \tag{28}$$

At the exterior surface of the arrester, at $x = \ell$, the primary mode of heat loss is through radiation to the ambient environment at temperature T_0(= 288 K). This particular choice of T_0 represents only one possible mine environment temperature. The radiative exchange is

moderated by an emissivity e_g for the gas and e_s for the solid. At $x = \ell$, the boundary condition for the gas temperature T_g is

$$-\lambda_g \frac{\partial T_g}{\partial x} = e_g \sigma (T_g^4 - T_0^4) + h (T_g - T_s), \quad (29)$$

and for the solid,

$$-\lambda_s \frac{\partial T_s}{\partial x} = e_s \sigma (T_s^4 - T_0^4) - h (T_g - T_s). \quad (30)$$

Initially, the arrester is at ambient temperature T_0 in the absence of a pressure differential. The increase in gas pressure P within the enclosure following the explosion is approximated as a linear rise over a small fraction of the time τ, followed by a linear decrease until τ has elapsed.

As discussed above, the competing thermal effects in equations 15 and 16 result in a wide variation in the time constants that are associated with the various modes of heat transport. This requires detailed computations so as not to obscure the physical processes. As part of the computational procedure, a finite difference representation of the partial differential equation was developed. Because of the possibility of steep spatial gradients in the gas temperature T_g and solid temperature T_s, a fine spatial mesh is required near the flame arrester exit. One approach is the application of a fine spatial mesh across the entire arrester. However, this approach can be computationally expensive. A second approach is to develop the finite difference equations over a nonuniform grid. This approach, while computationally less costly than a finely resolved uniform mesh, is first-order accurate compared with the second-order accuracy of the uniform spatial mesh. A third approach, which maintains the second-order spatial accuracy, yet provides more detailed information in spatial regions where the temperature gradient is steep, is an exponential coordinate transformation (*13*). This approach requires a transformation of the transport equations. Although the transformed equations are more complex, they are solvable in a regular mesh with constant grid spacing. This approach is the one selected for utilization of the model in this section.

An application of the exponential stretch coordinate transformation provides the user with a choice of defining in which region the grid has the finer resolution. In this application, the steepest temperature gradient occurs at the arrester exit, at $x = \ell$. Consequently, the transformation is written in the following form:

$$x = \beta (e^{-s} - 1), \quad (31)$$

where the transformed spatial coordinate $s = (I - 1)\Delta s$ for spatial node index I (I = 1,2,..., N), N is the total number of spatial nodes, and Δs is the grid spacing in the regular mesh defined by the variable s. For selected values of N and Δs, β, the scaling parameter in the coordinate transformation, equation 31, is determined.

$$\beta = \ell / (e^{-s_1} - 1), \quad (32)$$

where s_1 = transformed spatial coordinate at Nth node $(N - 1)\Delta s$.

Equations 15 and 16 are transformed by equation 31 and an application of the chain rule for partial differentiation.

$$\frac{\partial T_g}{\partial t} = \frac{\alpha}{\beta^2} e^{2s} \left(\frac{\partial^2 T_g}{\partial s^2} + \frac{\partial T_g}{\partial s} \right) + \frac{v}{\epsilon} \frac{1}{\beta} e^s \frac{\partial T_g}{\partial s} - \hat{h}(T_g - T_s), \quad (33)$$

$$\frac{\partial T_s}{\partial t} = \frac{\alpha_s}{\beta^2} e^{2s} \left(\frac{\partial^2 T_s}{\partial s^2} + \frac{\partial T_s}{\partial s} \right) + \hat{h}_s (T_g - T_s). \quad (34)$$

The derivative boundary conditions in equation 28 are similarly transformed. On the enclosure side of the arrester,

$$\left. \frac{\partial T_g}{\partial s} \right|_{s=0} = \left. \frac{\partial T_s}{\partial s} \right|_{s=0} = 0, \qquad t > \tau. \quad (35)$$

The temperature boundary conditions at the arrester exit, as expressed by equations 29 and 30, are recast in the transformed coordinate system.

$$\lambda_g \frac{1}{\beta} e^s \frac{\partial T_g}{\partial s} = e_g \sigma (T_g^4 - T_0^4) + h (T_g - T_s), \quad (36)$$

$$\lambda_s \frac{1}{\beta} e^s \frac{\partial T_g}{\partial s} = \epsilon_s \sigma (T_s^4 - T_0^4) - h (T_g - T_s), \quad (37)$$

at $s = s_1$.

The transformed equations, 33 through 37, are represented by an implicit finite difference scheme. A central, spatial finite difference representation is used for evaluation of the partial derivatives with respect to transformed coordinate s, except for the convective term, for which an upwind difference scheme is used. The resultant coupled, nonlinear algebraic equations are solved with the Thomas algorithm (*10*) at time t.

The transformed model equations, 33 through 37, were used to simulate the temperature evolution in a 1.27-cm-thick RETIMET flame arrester across which a maximum gas pressure differential of 3.47 psig is established. This pressure is characteristic of a test performed at the Pittsburgh Research Center. The combustion gas pressure is assumed to increase to a maximum over a 40-ms period and subsequently decay to atmospheric pressure 400 ms after the combustion initiation. The combustion temperature T_f is assigned a value of 1,840 K, characteristic of 6.8% CH_4-air combustion.

In order to adequately explore the effect of the gas-solid heat transfer coefficient h, two sets of computations were undertaken. The first set of computations was for heat transfer to spherical elements, and the second set was for heat transfer to cylindrical elements. Equations 21 and 22 define the respective heat transfer coefficients. An element is understood in this application to be the basic repetitive geometric structure from which the arrester is formed.

A gas emissivity e_g of 0.2 and solid emissivity e_s of 1.0 were used in the external surface boundary conditions, equations 36 and 37. For both cylindrical and spherical elements, calculations were made with the model equations for element diameters D between 2 and 2,000 μm. For spherical elements, the calculated maximum gas temperature T_g and solid temperature T_s and time t of occurrence at the arrester exit are shown in table 6. Table 7 shows the results of similar calculations for an arrester composed of cylindrical elements.

Table 6.—Calculated maximum gas temperature T_g and solid temperature T_s at arrester exit for sperical elements

D, μm	Gas		Solid	
	T_g, K	t, ms	T_s, K	t, ms
2	1,190	400	1,190	400
20	1,120	400	1,120	400
200 ...	1,030	360	1,000	390
2,000 ..	1,070	280	860	380

Table 7.—Calculated maximum gas temperature T_g and solid temperature T_s at arrester exit for cylindrical elements

D, μm	Gas		Solid	
	T_g, K	t, ms	T_s, K	t, ms
2	1,150	400	1,150	400
20	1,080	380	1,070	400
200 ...	1,040	340	970	390
2,000 ..	1,120	270	840	380

The one-dimensional model with gas temperature T_g and solid temperature T_s in local thermal equilibrium predicted, for the initial gas pressure and its associated decay time, that a maximum temperature of 1,183 K would occur on the arrester external surface after 1.1 s has elapsed. This temperature is in close agreement with the result in table 6 for a 2-μm-diameter spherical element. As equations 21 and 22 demonstrate, the smaller the element diameter D, the larger the gas-solid heat transfer coefficient h. Localized thermal equilibrium of the gas and solid is equivalent to an infinitely fast heat transfer rate.

Two inferences arise from a comparison of the results in tables 6 and 7. One is that the maximum gas temperature T_g and solid temperature T_s occur at, or slightly earlier than, the time for expulsion of the hot gas. The second inference is that the larger gas-solid heat transfer coefficient h associated with the spherical elements results in maximum T_s, which is only slightly higher than those associated with cylindrical elements.

Figure 4 shows the evolution of the gas temperature T_g and solid temperature T_s of the arrester external surface for a gas-solid heat transfer coefficient h defined for 200-μm-diameter cylindrical elements. T_g and T_s increase and decrease at approximately the same rate. Thermal energy is transferred from the gas to the solid during the expulsion of the hot gas. After that process is completed, the solid cools less rapidly than the gas at the external surface of the arrester because the thermal storage capacity of the arrester solid matrix is greater than the gas thermal storage capacity.

The results in tables 6 and 7 show that, although the gas-solid heat transfer coefficient h increases monotonically with decreasing element diameter D as shown by equations 21 and 22, the maximum gas temperature T_g does not vary monotonically with D. If the results in tables 6 and 7 are extended to the case of very inefficient gas-solid heat transfer from the gas to the solid mesh, which is simulated by the complete absence of convective heat transfer from the gas to the solid elements, T_g was shown to achieve a maximum value of 1,820 K simultaneously with the maximum value of gas pressure P at 40 ms. This temperature is only slightly less than the flame temperature T_f of 1,840 K. A slight increase in convective h to 10^{-4} cal·cm^{-2}·s^{-1}·K^{-1} resulted in a reduction in maximum T_g at the arrester external surface to 1,800 K at 40 ms and an increase in the maximum solid temperature T_s to 322 K at 400 ms. In each case, the energy loss at the arrester external surface is through radiation, which is the primary source of nonlinearity in the heat transport processes. These results indicate that an optimum gas-solid heat transfer is achievable, which would minimize maximum T_g and T_s at the arrester exit. This is an important consideration for arrester design.

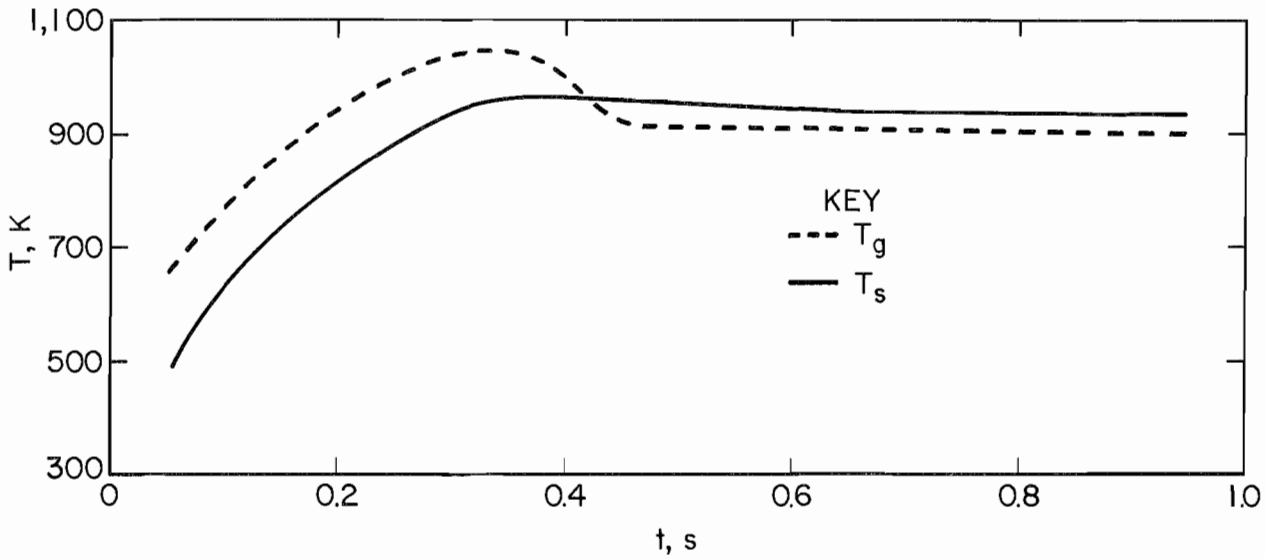

Figure 4.—Gas temperature T_g and solid temperature T_s at arrester exit over 1,000-ms period.

Further exploration with this model requires more detailed information regarding the internal structure of an arrester than is currently available. It is a viable model for arrester structure design provided the internal gas-solid heat transfer coefficient h can be defined. Without this information, it is reasonable to assume that the gas and solid are in local thermal equilibrium. An important consideration that has yet to be addressed is the heat loss from the arrester to the enclosure wall in which it is mounted. This heat transport process is accounted for by the development of a three-dimensional model in the following section.

THREE-DIMENSIONAL TRANSIENT THERMAL MODEL

The significant advantage of a three-dimensional thermal model is the capability to analyze the importance of lateral heat loss from the arrester into the wall in which it is mounted. This heat transport loss is of increased importance for small vent areas. It is assumed that the gas-solid convective heat transfer internal to the arrester mesh is rapid, and consequently, the gas and solid matrix are in local thermal equilibrium. As discussed previously in the "One-Dimensional Transients Thermal Models" section, this is a reasonable assumption for small-diameter mesh elements for which the gas-solid heat transfer rate is large.

The flame arrester is represented as a rectangular parallel piped in a three-dimensional coordinate system as shown in figure 5, with dimensions denoted by L, W, and H. The direction of gas flow is in x direction normal to y-z plane. In analogy to equation 10, the time-dependent thermal transport equation is a partial differential equation for the temperature T.

$$\frac{\partial T}{\partial t} = \alpha_0 \left(\frac{\partial^2 T}{\partial x^2} + \frac{\partial^2 T}{\partial y^2} + \frac{\partial^2 T}{\partial z^2} \right) - \beta_0 \rho_g C_{p_g} v \frac{\partial T}{\partial x}. \quad (38)$$

The boundary condition at x = 0 and x = L are the same as applied to equation 10.

At the arrester contact with the wall, isothermal boundary conditions are imposed.

$$T(x, 0, z) = T(x, W, z) = T_w, \quad (39)$$

for $0 < z < H,\ 0 < x < L$

$$T(x, y, 0) = T(x, y, H) = T_w, \quad (40)$$

for $0 < y < W,\ 0 < x < L,$

where T_w is the wall temperature, which is assumed constant at 288 K for the calculations presented in this section.

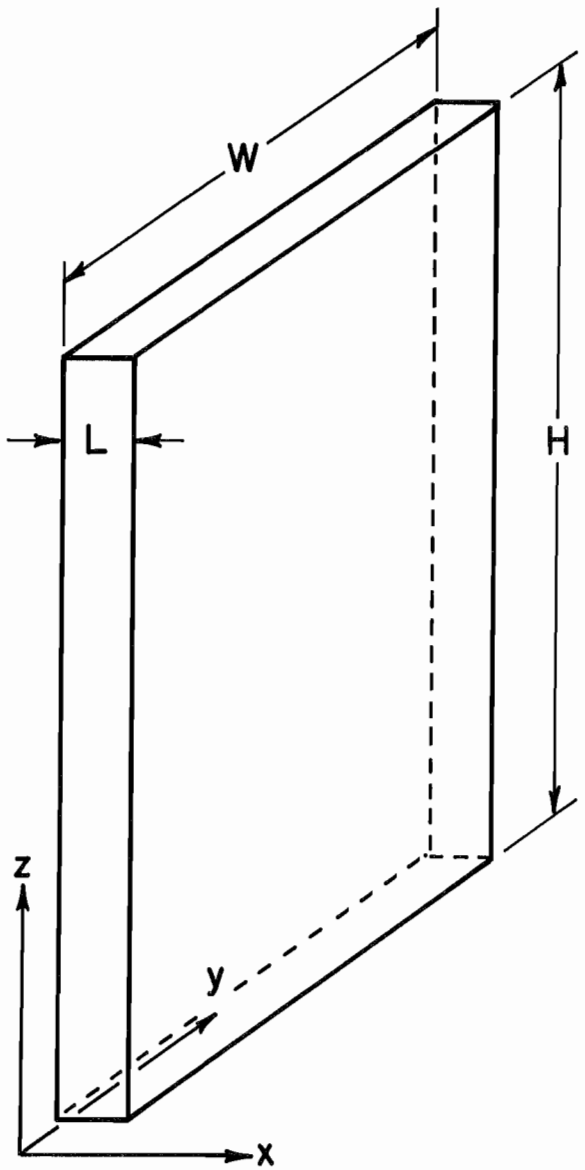

Figure 5.—Schematic of three-dimensional flame arrester.

In the absence of an explicit gas-solid heat transfer mechanism, the dominant rate-controlling mechanism is the convective heat transfer through the arrester defined by the time constant τ_2. The wide variation in the thermal time constants in the one-dimensional model with distinct gas and solid temperatures resulted in steep temperature gradients that required the implementation of an exponential stretched coordinate system. The numerical method for solving the model equation in this section, equation 38, is based upon a simpler computational algorithm. The implicit, central in space scheme used for the one-dimensional transient thermal model was expanded to three spatial dimensions. An iterative solution of the finite difference equations and the boundary conditions is developed over a small time increment to establish the time evolution of the temperature. Within a single iteration, the implicit in time, central in space finite difference representation of equation 38 is solved with the Thomas algorithm (*10*). The numerical procedure is listed as a FORTRAN computer program in appendix B.

The venting conditions described by the data in table 4 for a vent-area-to-enclosure-volume ratio of 28 $in^2 \cdot ft^{-3}$ were modeled with the three-dimensional code. For this particular application, the surface width and breadth were 1.625 and 8.75 in, respectively. Geometric and physical symmetry of the arrester permits analysis of a quarter section of the arrester to provide a temperature history of the entire arrester. In the nomenclature of figure 5, the quarter section is defined by

$$0 < y < 0.5W, \tag{41}$$

$$0 < z < 0.5H, \tag{42}$$

for $0 < x < L$.

Along the two internal sides of the quarter section, heat flow is absent because of symmetry. This is expressed as the following boundary condition:

$$\frac{\partial T}{\partial y} = 0,\ 0 < x < L,\ y = 0.5W,\ 0 < z < 0.5H, \tag{43}$$

$$\frac{\partial T}{\partial z} = 0,\ 0 < x < L,\ 0 < y < 0.5W,\ z = 0.5H. \tag{44}$$

The flame temperature T_f was assigned the value of the maximum inside surface temperature of the arrester, 1,274 K (1,001° C). A gas pressure relaxation time τ of 300 ms was assigned to the initial pressure differential of 0.37 psig. The outside surface temperature of the arrester at the geometric center of the arrester is shown in figure 6 over a 70-s period subsequent to the initiation of CH_4-air explosion. Shown for comparison is the outside surface temperature of the arrester for the one-dimensional model. As expected, the three-dimensional model prediction shows a slightly steeper temperature decrease than the one-dimensional model prediction. This is expected because of the lateral conductive heat loss in the three-dimensional model. For the three-dimensional model, the predicted maximum temperature of the arrester has a value of 249° C and occurs after 20 s has elapsed. This temperature is in moderate agreement with the measured value of 194° C reported in table 4, and exhibits a slightly better comparison than the value of 275° C determined from the one-dimensional model. The maximum

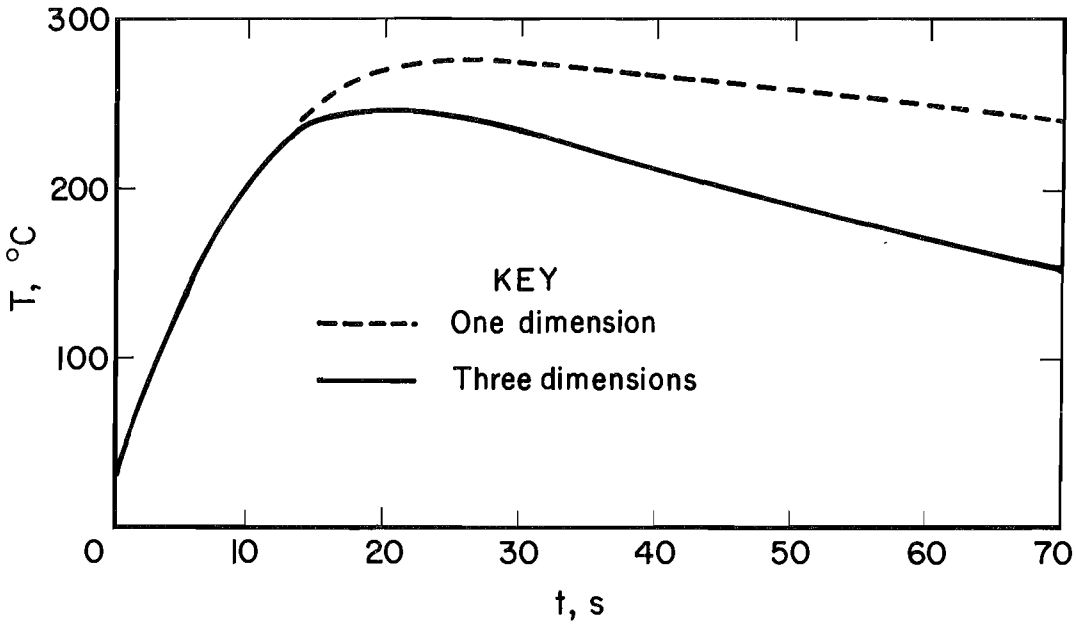

Figure 6.—Outside surface temperature of arrester for 0.37-psig overpressure that decays over 300-ms period and combustion temperature T_f of 1,001° C for one- and three-dimensional models.

outside surface temperature of the arrester occurs considerably later than the time required for expulsion of the hot gas. This time lag represents the time required for the thermal wave to traverse the arrester. In each case, the temperature decay of the arrester surface temperature is a slow process. Although the external surface temperature of the arrester is less than the ignition temperature for a combustible CH_4-air mixture (605° C), it is adequate to ignite coal dusts. The ignition time for a coal dust layer can require several minutes duration (*9*, p. 54). In view of the long thermal decay time of the arrester, this represents a potential hazard if coal dust settles on the arrester surface following the expulsion of the hot product gases and there is inadequate lateral heat loss to the enclosure walls.

Figure 7 shows the predicted temperature at nine discrete locations in a symmetric quarter section of the arrester after 20 s has elapsed. As expected, there is a temperature gradient across the arrester surface toward the wall support, which is at 15° C. In the lower left corner of the quadrant shown in figure 7, at a location 0.34 cm in y direction and 1.85 cm in x direction from the edges, the arrester surface temperature is 92° C.

Although information was not available with regard to the vent linear dimensions, width and length, for the three additional cases reported in table 4, an attempt to approximate the case in table 4 corresponding to the greatest maximum gas pressure P of the four cases was undertaken. This case represents a vent-area-to-enclosure-volume ratio of 12 $in^2 \cdot ft^{-3}$. The maximum gas pressure differential is 1.3 psig and the maximum inside surface temperature of the arrester is 1,411 K (1,138° C). It was assumed that one of the linear dimensions remained at 1.625 in, and consequently, the other linear cross-sectional dimension was decreased to 3.7 in. In contrast to the above case, the maximum temperature of the arrester outside surface increased to 538° C, but occurred at the earlier time t of 8 s. The predicted maximum temperature of 538° C is in only slightly closer agreement with the measured value of 358° C (shown in table 4) than the value of 551° C predicted by the one-dimensional model. The time evolution of the outside surface temperature of the arrester at the geometric center is shown in figure 8. A comparison with the case presented in figure 6 for the vent-area-to-enclosure-volume ratio of 28 $in^2 \cdot ft^{-3}$ shows a similar pattern to the temperature rise and decay.

The predicted maximum outside surface temperature of the arrester with the three-dimensional model for the 12 and 28 $in^2 \cdot ft^{-3}$ vent-area-to-enclosure-volume ratios are in closer agreement with the measured results than the results from the one-dimensional model. Table 8 shows a comparison of the predicted maximum outside surface temperature of the arrester based upon the one- and three-dimensional transient heat transport models, along with the measured values. The somewhat closer agreement of the maximum surface temperature predicted by

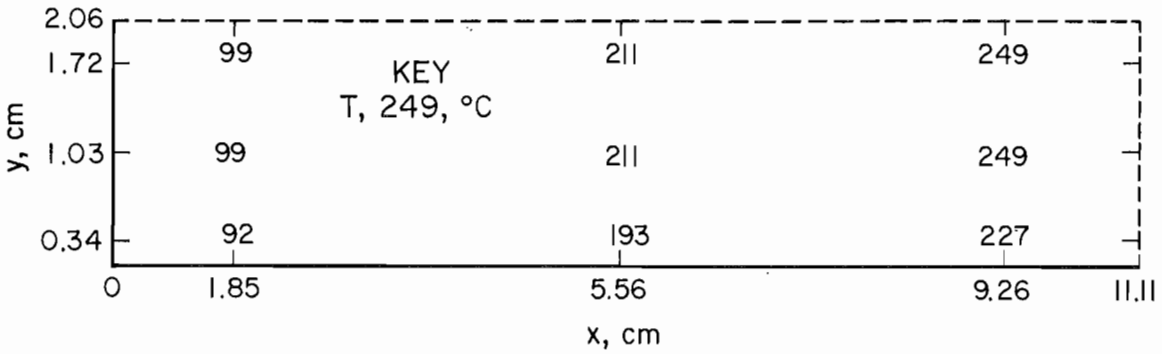

Figure 7.—Outside surface temperature at selected locations on quarter section of arrester surface after 20 s has elapsed for 0.37-psig overpressure that decays over 300-ms period and combustion temperature T_f of 1,001° C.

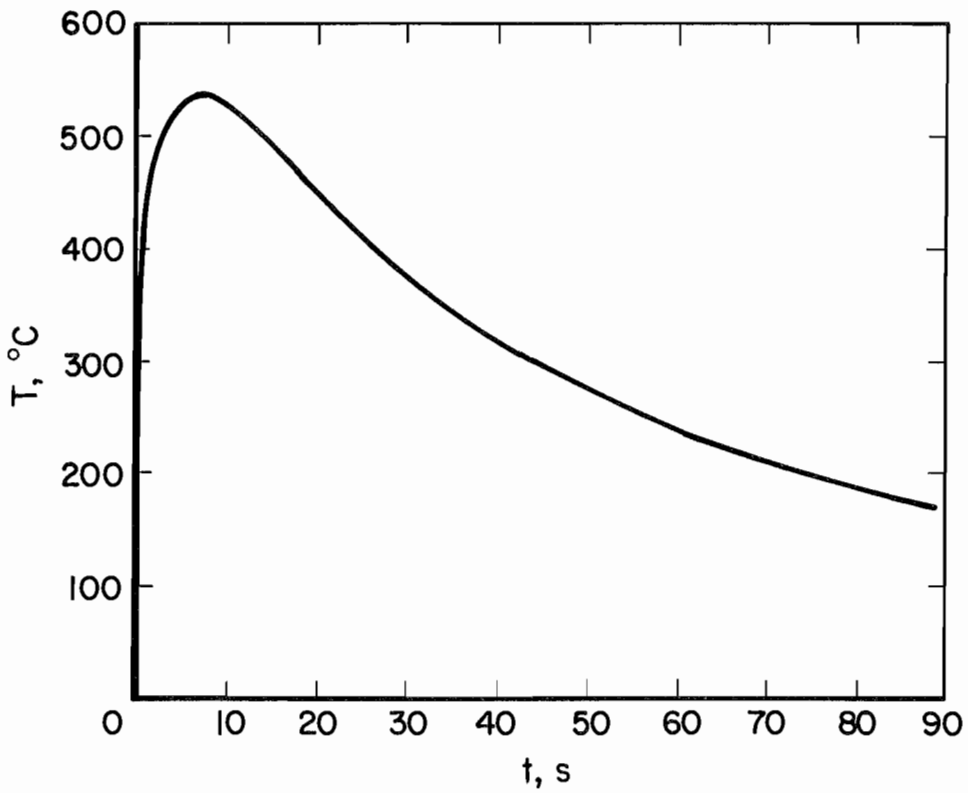

Figure 8.—Outside surface temperature of arrester for 1.3-psig overpressure that decays over 300-ms period and combustion temperature T_f of 1,001° C.

the three-dimensional model with the measured maximum temperature of the three-dimensional model is attributable to the lateral heat loss from the arrester edge to the isothermal wall. There is a degree of uncertainty inherent in this analysis because of the lack of information regarding the actual linear dimensions of the arrester surface for the vent-area-to-enclosure-volume ratio of 12 in^2-ft^{-3}. The predicted maximum temperature averaged over the arrester outside surface would be lower than the values reported in table 8 for the three-dimensional model as a consequence of the temperature gradient over the surface.

Table 8.—Measured and predicted maximum outside surface temperatures T, degree Celsius, of RETIMET flame arrester for vent-area-to-enclosure-volume (A/V) ratios between 12 and 28 in^2-ft^{-3}

A/V, in^2-ft^{-3}	Measured	1-D model	3-D model
12	358	551	538
28	194	275	249

CONCLUSIONS

Several thermal models of a flame arrester were developed, based upon the principles of heat transfer, that can be used to predict the maximum temperature a flame arrester can achieve when hot combustion gases are expelled through the arrester. The simplest model is a thermal equilibrium model. This model is an adiabatic model that provides a prediction of the maximum temperature the arrester can achieve, with or without metal screens present to extract heat from the expelled gases.

A more realistic representation of the maximum temperature a flame arrester can achieve was obtained from several transient heat transport models. These models were one- and three-dimensional transient models that include conductive, convective, and radiative heat transfer. The temperature evolution throughout the arrester was modeled. For the one-dimensional model with gas and arrester metal foam in local thermal equilibrium, the predicted maximum outside surface temperature of a RETIMET flame arrester showed an approximate agreement with the measured values for vent-area-to-enclosure-volume ratios between 12 and 28 $in^2 \cdot ft^{-3}$. The significance of radiative cooling was demonstrated. Extension of this model to three spatial dimensions included lateral heat loss across the arrester to the enclosure wall. An application of this model to a RETIMET flame arrester with a vent-area-to-enclosure-volume ratio of 28 $in^2 \cdot ft^{-3}$ showed a slightly more favorable comparison than did the one-dimensional prediction.

The one-dimensional model was further extended to distinguish gas temperature T_g and arrester metal foam temperature. This model is based upon a finite linear heat transfer rate between the gas and the arrester. It was demonstrated that there exists an optimum choice for the gas-solid heat transfer coefficient h that minimizes maximum gas temperature T_g and solid temperature T_s at the arrester exit. Currently, there is not sufficient information to precisely define h.

Each of these models can be used in the evaluation of the performance of existing flame arresters and in a parametric study that would support the design of a more efficient flame arrester.

REFERENCES

1. Scott, L. W. Vented Explosion-Proof Enclosure Research, Paper in Conference Record of the 1989 IEEE Industry Applications Society Annual Meeting, Part II (San Diego, CA, Oct. 1-5, 1989). IEEE Ind. Appl. Soc., 1989, pp. 1533-1535.

2. Ministry of Labour, Safety, Health and Welfare. Guide to the Use of Flame Arresters and Explosion Reliefs. H. M. Stationery Off. (London), New Ser. No. 34, 1965, 55 pp.

3. Gunderman, R. J. Innovations for Explosionproof Electrical Enclosures (contract H0357107, Dresser Ind., Inc.). BuMines OFR 121-81, 1980, 209 pp.; NTIS PB 82-104936.

4. Scott, L. W. Vented Explosion-Proof Enclosure Research. Paper in Proceedings of the Ninth WVU International Mining Electrotechnology Conference (Morgantown, WV, July 26-29, 1988). WV Univ., 1988, pp. 79-83.

5. Bradley, D., and A. Mitcheson. The Venting of Gaseous Explosions in Sperical Vessels. I—Theory. Combust. and Flame, v. 32, 1978, pp. 221-236.

6. Cooper, M. G., M. Fairweather, and J. P. Tite. On the Mechanisms of Pressure Generation in Vented Explosions, Combust. and Flame, v. 65, 1986, pp. 1-14.

7. Lunn, G. A. Methods for Sizing Dust Explosion Vent Areas: A Comparison When Reduced Explosion Pressures Are Low. J. Loss Prev. Process Ind., v. 2, Oct. 1989, pp. 200-208.

8. Conti, R. S., and M. Hertzberg. Thermal Autoignition Temperature for Hydrogen-Air and Methane-Air Mixtures. J. Fire Sci., v. 6, Sept.-Oct. 1988, pp. 348-355.

9. Kuchta, J. M. Investigation of Fire and Explosion Accidents in the Chemical, Mining and Fuel-Related Industries—A Manual. BuMines B 680, 1985, 84 pp.

10. Ames, W. F. Numerical Methods for Partial Differential Equations. Barnes & Noble, Inc. (New York), 1969, pp. 52-53.

11. Bird, R. B., W. E. Stewart, and E. N. Lightfoot. Transport Phenomena. Wiley, 1966, pp. 408-409.

12. McAdams, W. H. Heat Transmission. McGraw-Hill (London), 1942, p. 220.

13. Roache, P. J. Computational Fluid Dynamics. Hermosa Publ. (Albuquerque, NM). 1976, pp. 292-295.

APPENDIX A.—NOMENCLATURE

A	cross-sectional area of arrester, cm^2
a_k	ratio of m_k to m_{CH_4} for species k (k = CO_2, H_2O, and O_2), 1
A_s	cross-sectional area of screen, cm^2
C_{p_g}	constant pressure specific heat of gas, $cal \cdot g^{-1} \cdot K^{-1}$
C_{p_s}	constant pressure specific heat of arrester, $cal \cdot g^{-1} \cdot K^{-1}$
C_{p_l}	constant pressure specific heat of screen, $cal \cdot g^{-1} \cdot K^{-1}$
C_{v_k}	constant volume specific heat of gas for species k (k = CO_2, H_2O, and air), $cal \cdot g^{-1} \cdot K^{-1}$
D	element diameter, cm
d	wire diameter of screen, cm
e	emissivity, 1
e_g	gas emissivity, 1
e_s	solid emissivity, 1
f	CH_4-air mass fraction, 1
H	length in z direction of three-dimensional arrester, cm
h	gas-solid heat transfer coefficient, $cal \cdot cm^{-2} \cdot s^{-1} \cdot K^{-1}$
$\hat{h}$	coefficient in gas-solid heat transport equation, s^{-1}
$\hat{h}_s$	coefficient in solid heat transport equation, s^{-1}
I	index for spatial node, 1
L	length in x direction for three-dimensional arrester, cm
ℓ	arrester thickness, cm
ℓ_s	separation distance of screen wire, cm
m	arrester mass, cm
m_a	air mass, cm
m_{CH_4}	CH_4 mass, g
m_{CO_2}	CO_2 mass, g
m_{H_2O}	H_2O mass, g
m_{O_2}	O_2 mass, g
m_k	species k mass, g
m_s	screen mass, g
N	number of spatial nodes, 1
n	number of screens, 1
P	gas pressure, $dyn \cdot cm^{-2}$
P_1	gas pressure of external environment, psig
P_2	gas pressure in enclosure, psig
Pr	Prandtl number, 1
Re	Reynolds number, 1
R_g	molar gas constant, 8.3143×10^7 $erg \cdot mol^{-1} \cdot K^{-1}$
s	transformed spatial coordinate, 1
s_1	transformed spatial coordinate, at Nth node, 1
S_v	arrester-internal-surface-to-volume ratio, $cm^2 \cdot cm^{-3}$
T	temperature, K
T_g	gas temperature, K
T_s	solid temperature, K
t	time, s
T_f	flame or combustion temperature, K
T_0	ambient temperature, K
T_w	wall temperature, K
T_1	equilibrium temperature, K
V	enclosure volume, cm^3
v	superficial gas velocity, $cm \cdot s^{-1}$
W	length in y direction of three-dimensional arrester, cm
W_a	air molecular weight, $g \cdot mol^{-1}$
W_{CH_4}	CH_4 molecular weight, $g \cdot mol^{-1}$
W_g	gas molecular weight, $g \cdot mol^{-1}$
x, y, z	linear dimensions, cm
α	thermal diffusivity in gas-solid heat transport equation, $cm^2 \cdot s^{-1}$
α_s	thermal diffusivity in solid heat transport equation, $cm^2 \cdot s^{-1}$
α_0	thermal diffusivity in energy transport equation, $cm^2 \cdot s^{-1}$
β	scaling parameter in coordinate transformation, cm
β_0	parameter in energy transport equation, $cm^3 \cdot K^{-1} \cdot cal^{-1}$
ΔH_c	constant volume heat of combustion, $kcal \cdot g^{-1}$
Δs	grid spacing in transformed mesh, 1
ϵ	arrester porosity, 1
ϵ_s	screen porosity, 1
λ_g	gas thermal conductivity, $cal \cdot cm^{-1} \cdot s^{-1} \cdot K^{-1}$
λ_s	arrester thermal conductivity, $cal \cdot cm^{-1} \cdot s^{-1} \cdot K^{-1}$
μ	dynamic gas viscosity, $g \cdot cm^{-1} \cdot s^{-1}$
ρ_g	gas density, $g \cdot cm^{-3}$
ρ_s	arrester bulk density, $g \cdot cm^{-3}$
σ	Stefan-Boltzmann constant, 1.3551×10^{-12} $cal \cdot cm^{-2} \cdot s^{-1} \cdot K^{-4}$
σ_s	screen bulk density, $g \cdot cm^{-3}$
τ	gas pressure relaxation time, s
τ_1	time constant for gas-solid heat transfer, s
τ_2	time constant for convective heat transfer, s
τ_3	time constant for solid conduction, s
τ_4	time constant for gas conduction, s

APPENDIX B.—COMPUTER PROGRAM

DISCLAIMER OF LIABILITY

The U.S. Bureau of Mines expressly declares that there are no warranties expressed or implied that apply to the software described herein. By acceptance and use of said software, which is conveyed to the user without consideration by the Bureau of Mines, the user hereof expressly waives any and all claims for damage and/or suits for or by reason of personal injury, or property damage, including special, consequential, or other similar damages arising out of or in any way connected with the use of the software described herein.

```
      INCLUDE 'SUPPRSD.COM'
      LP=6
      MAX=1700
      MOP=25
      EPS=1.0E-05
      CALL INIT
      CALL PRES
      TMAX=T0
      JPP=-1
      KPP=-1
      NCTX=0
      TYMX-0.
      TIME=0.
      BETA=DT/DX/DX
      BETB=DT/DY/DY
      BETC=DT/DZ/DZ
      GAMA=DT/2./DX
      NCT=0
      IFLAG=0
      CALL OUTPT
 1000 CONTINUE
      IF(NCT.GT.600.AND.IFLAG.EQ.0) THEN
        DT=0.1
        BETA=DT/DX/DX
        BETB=DT/DY/DY
        BETC=DT/DZ/DZ
        GAMA=DT/2./DX
C       MOP=50
        IFLAG=1
      ENDIF
      IF(NCT.GT.800) THEN
        DT=0.1
        BETA=DT/DX/DX
        BETB=DT/DY/DY
        BETC=DT/DZ/DZ
        GAMA=DT/2./DX
        MOP=100
      ENDIF
      NCT=NCT+1
      MCT=0
 1200 CONTINUE
      MCT=MCT+1
      CALL PRES
      DO   50 J=2, M1
```

```
      DO    60 K=2, L1
      CALL COEF(J,K)
      CALL COEFP(J,K)
      CALL ALG(J,K)
60    CONTINUE
50    CONTINUE
      CALL BNDY
      IF(MCT.LT.7) GO TO 1200
      TEST=0.
      DO    100 I=1,N
      DO    120 J=1,M
      DO    140 K=1,L
      TEST1=ABS(TN(I,J,K)-TX(I,J,K))
      IF(TEST1.GT.TEST) THEN
         IX=I
         JX=J
         KX=K
         TEST=TEST1
      ENDIF
      TX(I,J,K)=TN(I,J,K)
140   CONTINUE
120   CONTINUE
100   CONTINUE
      IF(MCT.GT.195) WRITE(LP,990) NCT,MCT,IX,JX,KX,TEST,
     1 TN(IX,JX,KX)
990   FORMAT(/4X,'NCT,MCT,IX,JX,KX,TEST,TN:',5(2X,I4),2(2X,E12.5))
      IF(MCT.EQ.200) CALL OUTPT
      IF(MCT.EQ.200) STOP 'NONCONVERGENCE'
      IF(TEST.GT.EPS) GO TO 1200
      IF(MOD(NCT,MOP).EQ.0) CALL OUTPT
      DO    600 I=1,N
      DO    620 J=1,M
      DO    640 K=1,L
      T(I,J,K)=TN(I,J,K)
      TX(I,J,K)=TN(I,J,K)
640   CONTINUE
620   CONTINUE
600   CONTINUE
      TIME=TIME+DT
      DO    210 J=1,M
      DO    220 K=1,L
      IF(TN(N,J,K).GT.TMAX) THEN
         TMAX=TN(N,J,K)
         NCTX=NCT
         TYMX=TIME
         JPP=J
         KPP=K
      ENDIF
220   CONTINUE
210   CONTINUE
      IF(MOD(NCT,MOP).EQ.0) WRITE(LP,6000)  NCTX,TYMX,TMAX,JPP,KPP
      IF(NCT.EQ.MAX) THEN
         WRITE(LP,6000) NCTX,TYMX,TMAX,JPP,KPP
         STOP
      ENDIF
```

```
C       IF(TIME.LT.4.0*TAU) GO TO 1000
        IF(TIME.LT.1.0E+05) GO TO 1000
 6000   FORMAT(/4X,'NCTX,TYMX,TMAX,JPP,KPP:',2X,I5,2(2X,E12.5)
       1/4X,2(2X,I5)/)
        CALL OUTPT
        STOP
        END
        SUBROUTINE PRES
        INCLUDE 'SUPPRSD.COM'
        PWR=1./1.7
        P(N)=P1
        P(1)=FCN1(TIME)
        P(N)=FCN2(TIME)
        DO    100 I=1,N
        DO    125 J=1,M
        DO    150 K=1,L
        X=FLOAT(I-1)*DX
        P(I)=P(1)+(P(N)-P(1))/H*X
        RHO(I,J,K)=WM/RT*P(I)/T(I,J,K)
        PRS=((P(1)-P(N))/P0)*1000.
        U(I,J,K)=0.
        IF(TIME.LT.TAU) U(I,J,K)=(PRS*1.0/H/0.298)**PWR
C       U(I,J,K)=0.
C       U(I,J,K)=U(I,J,K)*TN(I,J,K)/T0
        U(I,J,K)=U(I,J,K)*100.
        W(I,J,K)=U(I,J,K)/POR
        V(I,J,K)=RHO(I,J,K)*CPG*U(I,J,K)/(POR*RHO(I,J,K)*CPG+(1.-POR)
       1            *RHOS*CPS)
        ALPHA(I,J,K)=XL0*T(I,J,K)/(POR*RHO(I,J,K)*CPG+(1.-POR)*RHOS
       1                  *CPS)
  150   CONTINUE
  125   CONTINUE
  100   CONTINUE
        RETURN
        END
        SUBROUTINE BNDY
        INCLUDE 'SUPPRSD.COM'
        DO    20 J=2,M1
        DO    40 K=2,L1
        TN(1,J,K)=TF
        IF(TIME.GT.TAU) TN(1,J,K)=TN(2,J,K)
C       TN(N)=TN(N-1)
        Z=TN(N,J,K)
        DO    100 NML=1,5
        F=Z**4-XL0/SIG/DX*T(N-1,J,K)*(TN(N-1,J,K)-Z)-T0**4
        DF=4.*Z**3+XL0/SIG/DX*T(N-1,J,K)
        Z=Z-F/DF
  100   CONTINUE
        TN(N,J,K)=Z
  40    CONTINUE
  20    CONTINUE
        DO    500 K=1,L
        DO    550 I=1,N
        TN(I,1,K)=FCT*T1+(1.-FCT)*TN(I,2,K)
C       TN(I,M,K)=FCT*T1+(1.-FCT)*TN(I,M-1,K)
```

```
      TN(I,M,K)=TN(I,M-1,K)
  550 CONTINUE
  500 CONTINUE
      DO   600 J=1,M
      DO   650 I=1,N
      TN(I,J,1)=FCT*T1+(1.-FCT)*TN(I,J,2)
C     TN(I,J,L)=FCT*T1+(1.-FCT)*TN(I,J,L-1)
      TN(I,J,L)=TN(I,J,L-1)
  650 CONTINUE
  600 CONTINUE
      RETURN
      END
      SUBROUTINE INIT
      INCLUDE 'SUPPRSD.COM'
      FCT=1.
      H=1.27
      D1=6.
      D2=6.
      D1=8.75
C     D1=3.7
      D2=1.625
      D1=D1*2.54
      D2=D2*2.54
      N=101
      N1=N-1
      N2=N-2
      N3=N-3
      M=15
      MA=(1+M)/2.
      M=MA-1
      M1=M-1
      M2=M-2
      M3=M-3
      L=15
      LA=(1+L)/2.
      L=LA-1
      L1=L-1
      L2=L-2
      L3=L-3
      INC=10
      DX=H/FLOAT(N-1)
      DY=0.5*D1/FLOAT(M1)
      DZ=0.5*D2/FLOAT(L1)
      CPS=0.158
      CPG=0.31
      SIG=1.355E-12
      RHOS=9.
      P0=1.01325E+06
      PM1=4.13
      PM2=1.44
      PM1=0.37
C     PM1=1.3
      PM2=0.
      PMAX1=P0*(1.+PM1/14.7)
      PMAX2=P0*(1.+PM2/14.7)
```

```
      TAU=0.3
      TAU1=0.03
      DT=TAU/400.
      P1=P0
      T0=288.
      T1=T0
      WM=29.
      RT=8.31451E+07
      RHO0=WM/RT*P0/T0
      TF=1274.
C     TF=1411.
      POR=0.95
      XLO=2.39E-06
      WRITE(LP,25) N,DX,H,POR,CPG,CPS,RHOS
 25   FORMAT(/4X,'N,DX,H,POR,CPG,CPS,RHOS:',2X,I4
     1,6(2X,E12.5)/)
      WRITE(LP,35) N,M,L,DX,DY,DZ,H,D1,D2
 35   FORMAT(/4X,'N,M,L,DX,DY,DZ,H,D1,D2:'/
     14X,3(2X,I5),6(2X,E12.5)/)
      WRITE(LP,50) PM1,PM2,TAU,P0,T0,TF,RHO0,XL0
 50   FORMAT(/4X,'PM1,PM2,TAU,P0,T0,TF,RHO0,XL0:'/
     18(2X,E12.5)/)
      WRITE(LP,75) FCT
 75   FORMAT(/4X,'FCT=',2X,E12.5/4X,'FCT=0 : ADIABATIC'/
     14X,'FCT=1 : ISOTHERMAL'/)
      DO   100 I=1,N
      DO   200 J=1,M
      DO   300 K=1,L
      TN(I,J,K)=T0
      T(I,J,K)=T0
      TX(I,J,K)=T0
      RHO(I,J,K)=RHO0
300   CONTINUE
200   CONTINUE
100   CONTINUE
      RETURN
      END
      SUBROUTINE COEF(JJ,KK)
      INCLUDE 'SUPPRSD.COM'
      J=JJ
      K=KK
      B(1)=(1.+2.*ALPHA(2,J,K)*(BETA+BETB+BETC))
      C(1)=(V(2,J,K)*GAMA-ALPHA(2,J,K)*(BETA      ))
      D(1)=T(2,J,K)+(V(2,J,K)*GAMA+ALPHA(2,J,K)*BETA)*TN(1,J,K)
     1        +ALPHA(2,J,K)*(BETB*(TN(2,J+1,K)+TN(2,J-1,K))
     2        +BETC*)TN(2,J,K+1)+TN(2,J,K-1)))
      DO   100 I=3,N2
      A(I-1)=-(V(I,J,K)*GAMA+ALPHA(I,J,K)*BETA)
      B(I-1)=1.+2.*ALPHA(I,J,K)*(BETA+BETB+BETC)
      C(I-1)=V(I,J,K)*GAMA-ALPHA(I,J,K)*BETA
      D(I-1)=T(I,J,K)
     1         +ALPHA(I,J,K)*BETB*(TN(I,J+1,K)+TN(I,J-1,K))
     2         +ALPHA(I,J,K)*BETC*(TN(I,J,K+1)+TN(I,J,K-1))
100   CONTINUE
      A(N-2)=-(V(N-1,J,K)*GAMA+ALPHA(N-1,J,K)*BETA)
```

```
      B(N-2)=1.+2.*ALPHA(N-1,J,K)*BETA+BETB+BETC)
      D(N-2)=-(V(N-1,J,K)*GAMA-ALPHA(N-1,J,K)*BETA)*TN(N,J,K)
     1          +T(N-1,J,K)+ALPHA(N-1,J,K)*(BETB*(TN(N-1,J+1,K)
     2          +TN(N-1,J-1,K))+BETC*(TN(N-1,J,K+1)+TN(N-1,J,K-1)))
      RETURN
      END
      SUBROUTINE COEFP(JJ,KK)
      INCLUDE 'SUPPRSD.COM'
      J=JJ
      K=KK
      CP(1)=C(1)/B(1)
      DP(1)=D(1)/B(1)
      DO   100 I=1,N3
      CP(I+1)=C(I+1)/(B(I+1)-A(I+1)*CP(I))
      DP(I+1)=(D(I+1)-A(I+1)*DP(I))/(B(I+1)-A(I+1)*CP(I))
  100 CONTINUE
      RETURN
      END
      SUBROUTINE ALG(JJ,KK)
      INCLUDE 'SUPPRSD.COM'
      J=JJ
      K=KK
      TN(N-1,J,K)=DP(N-2)
      DO   100 II=2,N2
      I=2+N2-II
      TN(I,J,K)=DP(I-1)-CP(I-1)*TN(I+1,J,K)
  100 CONTINUE
      RETURN
      END
      SUBROUTINE OUTPT
      INCLUDE 'SUPPRSD.COM'
      WRITE(LP,990) NCT,MCT,IX,JX,KX,TEST,
     1 TN(IX,JX,KX)
  990 FORMAT(/4X,'NCT,MCT,IX,JX,KX,TEST,TN:',5(2X,I4),2(2X,E12.5))
      WRITE(LP,100) NCT,TIME,DT,TEST,P(1),P(N)
  100 FORMAT(/4X,'NCT,TIME,DT,TEST,P(1),P(N):',2X,I6,5(2X,E12.5))
      WRITE(LP,200)
  200 FORMAT(/)
C     J=(1+M)/2
C     K=(1+L)/2
      MJ(1)=2
      MJ(3)=M-1
      MJ(2)=(1+M)/2
      DO   500 JJ=1,3
      J=MJ(JJ)
      DO   600 ILK=1,3
      K=2
      IF(ILK.EQ.2) K=(1+L)/2
      IF(ILK.EQ.3) K=L-1
      WRITE(LP,550) J,K
  550 FORMAT(/4X,'J,K:',2(2X,I5)/)
      WRITE(LP,300) (TN(I,J,K),I=1,N,INC)
  300 FORMAT(5(2X,E12.5))
      WRITE(LP,200)
      WRITE(LP,300) (U(I,J,K),I=1,N,INC)
```

```
      WRITE(LP,200)
      WRITE(LP,300) (RHO(I,J,K),I=1,N,INC)
      WRITE(LP,200)
      WRITE(LP,300) (P(I),I=1,N,INC)
      WRITE(LP,200)
      WRITE(LP,300) (V(I,J,K),I=1,N,INC)
      WRITE(LP,200)
      WRITE(LP,300) (ALPHA(I,J,K),I=1,N,INC)
      WRITE(LP,200)
      WRITE(LP,300) (TN(I,J,K),I=1,10)
      WRITE(LP,200)
      WRITE(LP,300) (TN(I,J,K),I=N-10,N)
      WRITE(LP,200)
      WRITE(LP,300) (U(I,J,K),I=1,10)
      WRITE(LP,200)
      WRITE(LP,300) (RHO(I,J,K),I=1,10)
      WRITE(LP,200)
      WRITE(LP,300) (P(I),I=1,10)
      WRITE(LP,200)
      WRITE(LP,300) (ALPHA(I,J,K),I=1,10)
      WRITE(LP,200)
      WRITE(LP,300) (V(I,J,K),I=1,10)
  600 CONTINUE
  500 CONTINUE
      RETURN
      END
      FUNCTION FCN1(X)
      INCLUDE 'SUPPRSD.COM'
      FCN1=PMAX1+(P0-PMAX1)/TAU*TIME
C     IF(TIME.LT.TAU1) FCN1=PMAX2+(PMAX1-PMAX2)/TAU*TIME
C     IF(TIME.GE.TAU1) FCN1=PMAX1+(P0-PMAX1)/(TAU-TAU1)*(TIME
C    1                              -TAU1)
      IF(FCN1.LT.P0) FCN1=P0
      RETURN
      END
      FUNCTION FCN2(X)
      INCLUDE 'SUPPRSD.COM'
      FCN2=PMAX2+(P0-PMAX2)/TAU*TIME
      IF(FCN2.LT.P0) FCN2=P0
      RETURN
      END
      IMPLICIT DOUBLE PRECISION (A-H,O-Z)
      PARAMETER IA=501,JA=21,KA=21
      COMMON/FLAME1/LP,NCT,MCT,TIME,DT,H,N1,N2,N3,N,DX,CPG,
     1              CPS,XL0,RHO0,RHO1,P0,T0,T1,TF,BETA,GAMA,
     2              PMAX1,PMAX2,MAX,MOP,INC,TAU,POR,P1,RT,WM,
     3              RHOS,TEST,SIG,TAU1,TMAX,NCTX,TYMX,BETB,BETC,
     4              M,M1,M2,M3,L,L1,L2,L3,DY,DZ,IX,JX,KX,FCT
      COMMOM/FLAME2/T(IA,JA,KA),TN(IA,JA,KA),TX(IA,JA,KA),P(501),
     1              RHO(IA,JA,KA),U(IA,JA,KA),ALPHA(IA,JA,KA),
     2              V(IA,JA,KA),A(501),B(501),
     3              C(501),D(501),CP(501),DP(501),W(IA,JA,KA),MJ(5)
```

☆ U.S. GPO: 1991—511-010/42,013 INT.BU.OF MINES,PGH.,PA 29405